Exercise and the brain: a mechanical model for pulsation on flow of cerebrospinal fluid

Michael G. Hale[1] and Jonathan A. Coles[2]
[1]School of Physical Sciences, The Open University, Walton Hall, Milton Keynes, MK7 6AA.
[2]Centre for Immunobiology, Institute of Infection, Immunity and Inflammation, College of Medical, Veterinary and Life Sciences, University of Glasgow, Sir Graeme Davies Building, 120 University Place, Glasgow, G12 8TA, United Kingdom.

Correspondence: jonathan.coles@glasgow.ac.uk

Abstract.
Exchange of molecules between cerebrospinal fluid (CSF) and brain cells contributes to brain function and protection from dementia, but the route by which CSF is brought close enough to the neural tissue to be exchanged by extracellular diffusion is not clear. Exogenous molecules injected into CSF are carried along channels outside arteries and reach the basement lamina that surrounds the dense capillary network. Transport of solutes by diffusion along the basement lamina, a gel of macromolcules about 100 nm thick, would be too slow; bulk flow in a static geometry would require unphysiologically high pressures. However, it is known that the pulsation of blood aids transport of CSF, and we hypothesized that this is because the pulsation intermittently squeezes the pericapillary lamina. In a primitive mimicry, we have tested whether intermittent squeezing increases flow through an agar gel. In all but one of 216 tests, pulsation caused a reversible increase, sometimes by a factor of 100 or more. The enhancement was greatest for frequencies 5-11 Hz and, over the tested range of pressure heads (20 - 50 cmH_2O), was greatest for the lowest pressure. The results suggest one reason why exercise slows the aging of the brain.

Keywords: Brain; mouse; gel; perivascular space; Darcy's Law; basal lamina.

1. Introduction.

1.1. Details of how CSF irrigates brain tissue are unknown.

Blood supplies the main molecules required for brain metabolism, glucose and oxygen. Arterioles penetrating into the brain from the surface carry blood to a dense capillary network drained by venules that return it to veins on the brain surface (Fig. 1(*a*-*c*)). Glucose and oxygen can escape across the capillary wall and then diffuse the short distances (on average 13 µm, [1, 2] to the neurons and glial cells. A second, complementary, source of other necessary molecules, including vitamins and DNA precursors, is cerebrospinal fluid (CSF) (reviewed by [3, 4]). CSF can also carry away molecules, such as amyloid beta, whose accumulation in the brain is associated with Alzheimer's disease [5]. CSF is secreted into the brain ventricles by the choroid plexuses which synthesize, or transport from blood, a palette of molecules. By injecting marker molecules visible in microscopy it has been shown that CSF flows through ducts connecting the ventricles to the surface of the brain at the cisterna magna and from there is distributed to the surface of the cortex [6-12]. Although they

have been discussed for over a century [13], the pathways that then bring CSF close enough to the neurons and glial cells for molecules to be exchanged with them by diffusion alone are still debated (e.g., [4]). It is generally agreed that CSF flows down a perivascular space of the arterioles that leave the cortical surface and penetrate into the neural tissue (Fig. 1(*c*); [4]). It has been strongly argued that CSF then crosses a layer of astrocyte endfeet that delimit the perivascular space and moves by bulk flow through the extracellular matrix of the neural tissue to reach the perivascular space of venules; this is called the 'glymphatic' system [9, 14]. From the perivenular space CSF follows the venules back up to the brain meninges and, at normal intracerebral pressures, most of it leaves the cranium through the foramina (holes) that carry blood vessels or nerves [15-18].

An objection that has been made to the glymphatic theory is that bulk flow through the extracellular matrix would require unphysiologically high pressure gradients [12, 19-21]. Another possible weak point is that it has repeatedly been observed that molecules carried by CSF are found, concentrated relative to adjacent tissue, in the basement lamina that surrounds brain capillaries (Fig. 1(b); [7, 22, 23] [9, 10]. As stated by [7, 23-26] this observation tends to support the declaration by Cathélin (1903, ref. [13]) that CSF molecules are transported from peri-arteriolar space to perivenular space along conduits adjacent to the capillaries. Since current intravital imaging techniques lack the resolution needed to clearly image the capillary basement lamina (which is about 100 nm thick) these results were obtained on tissue chemically fixed after death. It has been objected that CSF reaches this location only after cardiac arrest, perhaps because of the sudden drop in blood pressure [27-29]. But, inevitably, control images of living capillaries are lacking. Bulk flow along a paracapillary route is attractive because it would allow the density of the capillary network to be exploited to bring CSF within diffusion distance of the neural cells. The major objection has been that there appears to be no space for liquid to flow freely adjacent to capillaries, all extracellular spaces being filled by a matrix of macromolecules [25, 30] as for the neural tissue itself ([12, 19-21], and adequate convective transport would be impossible without an unphysiologically large pressure gradient. At least if the geometry were static. Experiments have shown that delivery of CSF to pericapillary space in the brain and also maintainance of brain function are greatly reduced if the pulsation of the circulating blood is reduced [7, 31]. Analogous results have been found for bulk flow through the extracellular matrix of rabbit skin, and in skin it has been further shown that intermittent squeezing of the tissue increases bulk flow [32, 33]. Blood pulsation also appears to assist CSF flow along the paravascular spaces of cerebral arteries and veins ([9, 10, 29]. These observations have led us to ask if the pulsating pressure outside blood vessels caused by the pulsation of the blood supply might account for the repeated observation that CSF markers can reach the pericapillary 'space'.

We find no report of experiments on the effect on flow through a matrix of macromolecules in a defined geometry of applying pulsating lateral pressure changes. To see if pulsation is capable of affecting flow, we have started with an experimentally simple arrangement. We have measured the flow of salt solution through a column of gel in an elastic tube under a small static longitudinal pressure gradient and then applied repetitive lateral compression (Fig. 1(*d*)). We have examined the dependence of the flow on the degree of compression of the tube, the frequency of pulsation, and the static pressure head. Under the conditions we used, we found that pulsation reversibly increased the flow, sometimes by a factor of a hundred or more. We conclude that in the presence of a pulsating blood flow, bulk

paracapillary flow of CSF may be possible. This effect of blood pulsation may be one reason why physical exercise benefits the brain [34].

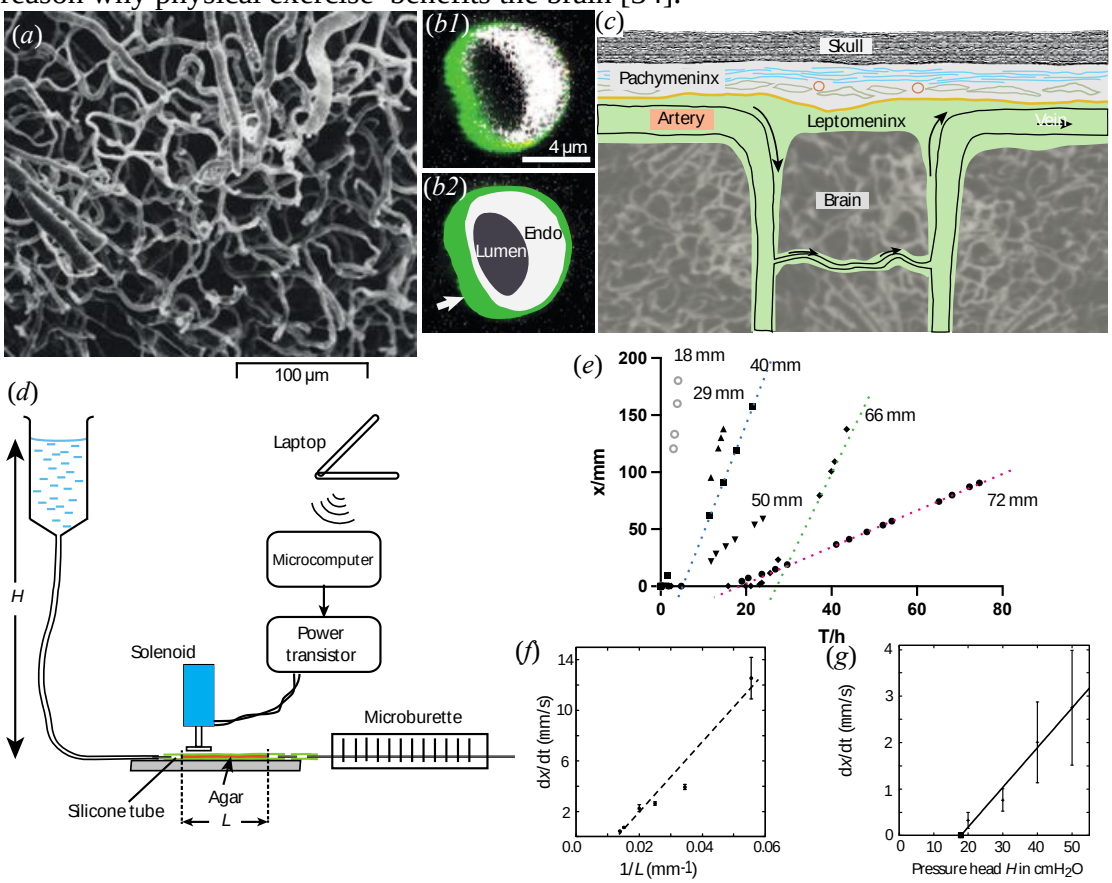

Figure.1. (*a*). A cast of the blood vessels in the cortex of a rat brain (modified from [2]). (*b1*) A CSF marker dye in a space surrounding a capillary in a section of fixed mouse brain. Endothelium is labelled by expression of GFP (shown in white) driven by the Tie-2 promoter. Ovalbumin conjugated with Alexa Fluor 647 (M.Wt. 45 kDa, shown as green) was injected in the cisterna magna less than 30 min before perfusion fixation (from Fig. 3C in [9] with permission). (*b2*) Interpretation of (*b1*) indicating the lumen of the capillary, its endothelial cell wall and (arrow) the basement lamina. (*c*) Scheme of the pathway of CSF in the cortex proposed by [7, 13, 25, 26, 35] showing flow of CFS along a pericapillary space. CSF flows in the subarachnoid space of the leptomeninx, the inner of the two meningeal compartments, which is separated from the outer compartment, the pachymeninx, which contains a layer of collagen (blue), the dura mater. (*d*) Minimal portrayal of the experimental set-up (see Supp Mat 1 for details). (*e*) Displacement, x, of the bubble in the microburette caused by flow through gel columns of different lengths L, with a static pressure gradient of 40 cm H_2O. (*f*) The mean flow rates for the linear parts of (*d*) plotted against $1/L$. (*g*) Flow rates through columns approximately 40 mm long at different pressure heads H. Bars are SEMs. The regression line through the data points does not extrapolate to zero.

2. Methods

2.1. Preparation of gel columns and the apparatus for pulsation

Silicone tubing, i.d. 1.0 mm, o.d. 3.0 mm, was cut into 40 - 80 mm lengths, filled with agar agar (Falooda powder, Top op Foods Ltd, UK), 1% w/v, prepared, and stored in, 0.15M NaCl. Five mm of gel was flushed from each end of a length of tube and it was connected upstream to a pressure head of 20 -50 cm H_2O and downstream to a microburette consisting of polyethylene tubing, i.d. 0.38 mm, held against a 200 mm scale (Fig. 1(*d*)). A small index bubble was introduced into the microburette so that the movement of fluid could be measured. The gel-filled tube was held under a

solenoid-driven piston, diameter 3.5 mm, that could pummel the tube at a frequency controlled by a microcomputer (Raspberry Pi zero) instructed by wifi from a laptop (SM2). The solenoid was mounted on a micromanipulator with a Vernier scale so that the approximate compression of the silicone tube could be controlled. Experiments were done at 18-22 °C. More details of the Methods are given in Supplementary Material 1.

2.2. Control Experiment: Periodic compression slowed the flow of water through a fluid-filled elastic tube.

Water with a head of about 30 cm flowed through a horizontal silicone tube, i.d. 1.0 mm, which passed beneath a small solenoid (Fig.SM2(*a*)). The flow was adjusted with a control valve to about 0.1 ml/sec. The water was switched to a coloured solution ($CuSO_4$) and changes in the optical density at a point downstream of the solenoid were monitored using a red LED and a photodiode (Fig. SM2(*b*)). Squeezing the tube at 2 - 5 Hz with the solenoid slightly reduced the flow, as might be expected as the lumen of the tube was constricted for part of the time (Fig. SM2(*c*)). Squeezing produced no marked difference in the time course of the progressive increase in optical density caused by the arrival of the solute.

3. Results.

3.1. Flow through the gel without pulsation

The volume flow, Q, through the column of 1% agar was measured by the displacement x of the bubble along the microburette scale. Results for six gel columns with lengths L = 18 - 72 mm at a pressure head H = 400 mm H_2O are shown in Fig. 1(*e*). The speed of displacement, dx/dt, was approximately constant for most of the observation period. There was often an initial period during which the bubble moved very slowly, so that extrapolation from the linear phase did not pass through the origin (dashed lines in Fig. 1(*e*)). When gel columns of different lengths were compared, the expected relationship $dx/dt \propto 1/L$ [36] was approximately observed (Fig. 1(*f*)). When the pressure head H was varied between 20 and 50 cm H_2O, flow rate increased with H at pressures beyond a threshold of about 182 mm H_2O (Fig. 1(*g*)). Such deviation from Darcy's Law at low pressures is an accepted feature of flow through porous mineral beds [37-40]. We calculated Darcy's permeability coefficient (the mean specific hydraulic conductivity, see [41])

$$K = Q\eta L / A\Delta P \qquad (1)$$

where Q is the volume flow, η is the viscosity of the fluid, taken as 1.06 mPa.sec [42], L is the length of the gel column, A is the cross-section of the silicone tube and ΔP is the pressure difference across the gel. $\Delta P = \rho g H$ where ρ is the density of the fluid, and H is the height of the reservoir above the gel. The data shown in Fig. 1(*g*) give a range of K of 3.9-10.1 x 10^{-16} m^2, with a mean of 7.6 x 10^{-16} m^2 . The SDs of individual measurements are in the order of the mean values.

3.2. Pulsation increased the flow

In all but one of more than 216 tests, periodic compression ('pulsation') of the silicone tube, with a duty cycle of 50%, reversibly increased the flow of water through the column of agar gel. Results from a typical experiment are shown in Fig. 2(*a*): in this experiment, pulsation at 1 - 15 Hz increased the flow by factors of 3 - 11. For small compression depths, up to 0.5 mm, the enhancement increased monotonically with compression depth (Fig. 2(*b*)); at greater compression depths no systematic trend was observed in the noise (not shown). If the pulsation was applied when the speed of the

index bubble was very small (< 1 mm/h, see Fig.1(*c*)), the apparent enhancement could be very great: values over one hundred were excluded from averages.

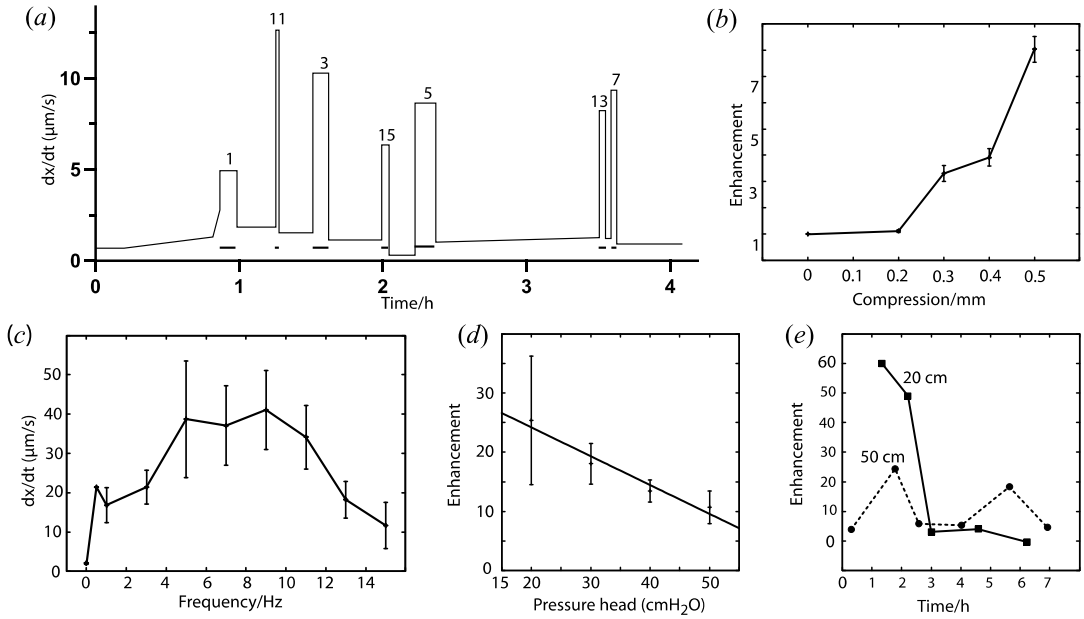

Figure 2. Pulsation increased flow through the gel. (*a*). Results from one gel column. The average speed between readings of the index bubble in the microburette is plotted against time. Bars indicate pulsation at the frequencies given in Hertz. *L* = 16 mm, *H* = 30 cm. (*b*). Enhancement of flow by pulsationsion at 2 Hz *vs* the compression by the solenoid. The data are for one gel column 30 mm long and a pressure head of 30 cm H_2O. One outlying data point (much greater enhancement) was excluded (*c*). Mean speed in the microburette as a function of pulsation frequency. Results on 10 gel columns with *L* = 38-41 mm, *H* = 40 cm. 6 -15 measurements per frequency (except for 0.5 Hz). Bars are SEMs: there was great variation between measurements. With no pulsation the flow rate was 2.03 ± 0.25 µm/s. (*d*) Mean flow enhancement vs pressure head at 5-11 Hz. Pooled results from a total of 55 measurement cycles with *L* = 16 - 53 mm, *f* = 5 - 11 Hz. (*e*)**.** Result from a single experiment in which *H* was alternated between 20 cm and 50 cm. Enhancement changed radically over tens of minutes. *L* = 30 mm, *f* = 7 Hz.

3.3. Dependence on frequency

Fig. 2(*c*) shows pooled results from ten gel columns of the speed of displacement of the index bubble. Bouts of pulsation at different frequencies were applied in pseudo-random order. Dividing *Q*(*f*) by the mean of the baselines, *Q*(0), just before and just after the pulsation, did not give a cleaner result, partly because in some cases the flow without pulsation was very small or undetectable.

3.4. Dependence on pressure head

Pooled results from 55 tests showed that with pressure heads ranging from 20 cm H_2O to 50 cm, the mean enhancement was greatest with *H* = 20 cm and fell as the pressure head was increased to 50 cm H_2O (P = 0.022, Fig. 2(*d*)).

3.5.Variability

Despite the trend in the pooled results of Fig. 2(*d*), in individual experiments great variability was observed. For example, in the extreme case shown in Fig.2(*e*), the enhancement with H = 20 cm H_2O was greater than that for 50 cm for some hours but switched to being less after 2.9h.

4. DISCUSSION

4.1. Characteristics of flow through agar without pulsation

We have found no previous measurements of the permeability of 1% agar. Our measurements gave a mean Darcy coefficient of 7.6 x 10^{-16} m^2 which is close to the value of 6.16 x 10^{-16} m^2 found for 2% agarose by [43], but 579 times less than that of [44] (4.4 x 10^{-13} m^2). The plot of bubble speed vs pressure head (Fig. 1(*g*)), shows that there was little or no flow at the lowest pressures, in qualitative agreement with results on flow through soil and fractured rock [37-40], and has been attributed to increased viscosity at the solid-liquid interface [45]. Previous experimenters have reported that flow could be initially very slow then increase after times in the order of minutes [43, 46]. We also observed delays which, at the lowest pressure gradients, could last for several hours (Fig. 1(*e*)). We have no explanation for this.

4.2. Flow through agar with pulsation

We have found no previous report of the effect of applied pulsation on flow through a gel (apart from experiments on skin [33]). The forces we applied were complex, with predominantly transverse compression under the solenoid, and longitudinal pulsation downstream: it is unlikely that this was an efficient application of compression. The control speed of the index bubble along the microburette (in the absence of pulsation) sometimes changed markedly after a period of pulsation (Fig. 2(*a*,*e*)) which indicates that pulsation could cause a persistent change in the resistance of the system. Because the interface between solid and liquid was far greater within the gel than in the microburette we suggest that the instability was within the gel column, rather than in the measuring system. This interpretation is supported by the observation that erratic changes in speed were far less evident in experiments with no pulsation (Fig. 1(*e*)). We offer no further explanation.

Averaged data showed that maximum flow was produced by pulsation in the range 3 - 13 Hz. This overlaps the range of heart rates in mice (6.6 - 13 Hz [47]) and is close to the range in humans (1 - 3 Hz). Since the area of fluid-solid interface, both within our gel model and in pericapillary tissue, is almost entirely within matrices of macromolecules, rather than at macroscopic solid surfaces, it is not far-fetched to suggest that physiological heart rates might well enhance flow through a basement lamina.

Averaged data also showed a significant tendency for pulsation-induced enhancement of bulk flow to decrease as the pressure head was increased over the tested range of 20 - 50 cmH_2O applied to a 40 mm column (Fig. 2(*d*)). As the pressure gradient decreases another process, transport of solutes by mixing, will play a greater role, much as described for the fluid in the PVS of penetrating arterioles [48, 49].

4.3. Relevance to a hypothetical flow along the pericapillary basement lamina

The pulsation of the penetrating arterioles [10] will produce pulsatile pressures on the capillary basement lamina at its proximal end. Venules downstream of brain capillaries are also observed to pulsate [10] indicating that the blood flow through the capillaries that feed into them is pulsatile. Unless the capillary endothelium is perfectly inelastic, this must result in some pulsatile compression of the basement lamina. Hence pulsatile compression of the basement lamina is a reasonable hypothesis. If the hydraulic conductivity of the pulsed lamina were similar to that of 1% agar, could it support transport of physiological fluxes of CSF under physiological

pressure gradients? The greater the CSF flux, the greater the forces needed to drive it so we conservatively consider the maximum possible CSF flux. Since it is not known how much of the CSF that reaches the leptomeninx then irrigates the neural tissue [4], we consider the extreme hypothesis that all CSF produced by the choroid plexuses is distributed to flow along paracapillary conduits: this both leads to the highest estimate of the pressure gradients required, and might be expected as a result of evolutionary selection. The rate of production of CSF in mouse is disputed: two reports give 0.33 - 0.37 µL/min [50, 51] whereas [52] give 0.1 µL/min. The the volume of the mouse brain is 0.43 cm^3 [53] so a high estimate of the production per unit volume is 0.86 µL min^{-1} cm^{-3}, which is similar to that in the rat ([54-57]. The total length of capillaries per unit volume of brain (in mouse, rat and cat) is about 1000 mm/mm^3 [1, 58-60] and the mean length of individual capillaries is about 100 µm [2]. Hence, there are 10^4 capillaries per mm^3 or 10^7 per cm^3 and the paracapillary flow of CSF along each capillary is

$$Q = 0.86 \times 10^{-7}\ \mu L/min = 1.4\ fL/s = 1.4 \times 10^{-18}\ m^3/s \qquad (2)$$

Taking the external diameter of a brain capillary as 4 µm [1, 58, 61] and the thickness of the basement lamina as 0.1 µm [62-64], the cross-section of the basement lamina of a capillary is

$$A = \pi \times (\text{diameter}) \times (\text{thickness})$$
$$= 4\pi \times 0.1\ \mu m^2 = 1.26\ \mu m^2 \qquad (3)$$

Speed of flow along basement lamina =

$$Q/A = 1.4 \times 10^{-18}\ m^3\ s^{-1} / (1.26 \times 10^{-12}\ m^2)$$
$$= 1.11\ \mu m/s \qquad (4)$$

The data in Fig. 2(*c*) show that for frequencies in the range of the mouse heart beat (7 - 12 Hz; [47] and a pressure gradient of 40 cm H_2O over 0.4 cm, dx/dt in the microburette ≈ 40 µm/s. Adjusting for the different diameter, the speed of flow in the agar column = 40 x $(0.38/1)^2$ µm/s = 5.78 µm/s. Making the approximation that Darcy's Law applies, so speed ∝ pressure gradient ([36], the pressure gradient needed for the speed through the agar gel to equal that along the basement lamina (Eq. (4)) is

$$\text{Pressure gradient} = 10 \times 1.11/5.78\ mmH_2O/mm = 0.193\ cmH_2O/mm \qquad (5)$$

Little is known about pressure gradients in the brain. Holter et al. [20] considered that the upper possible limit was 1.36 cmH_2O/mm, which is more than seven times the estimate in Equ. (5), and so could drive the hypothetical flow with a large margin.

More relevant is the pressure drop not in the neural tissue but between the CSF in the periarteriolar space at the upstream end of a capillary and the perivenular space at the downstream end: for a capillary with a typical length of 100 µm [2] the requirement would be 0.0193 cmH_2O. The pressure drop along the *inside* of a capillary can be as high as 34 cmH_2O [65] which is 1761 times as big. It is not clear to us how this might affect the basement lamina, but the energy necessary to compress it is available in the vicinity.

We conclude that although we do not know whether the effect of pulsation on the basement lamina causes greater or less enhancement of flow than the solenoid in our model, it would be rash to dismiss old [13] and recent [24-26] suggestions that CSF flows through a paracapillary pathway. In our model system, the transport increased with the frequency of pulsation over the range 0-5 Hz (Fig. 2(c)), and with the depth of compression, up to at least 1/6 of the external diameter of the gel-filled tube (Fig. 2(b)). An analogous progressive effect on the capillary baseent lamina

might account for the beneficial effect of physical exercise that involves increased cardiac output. This would complement other conditions that favour CSF distribution, such as slow-wave sleep [66].

Data accessibility. The code used to control the solenoid is available at https://github.com/GolfPapaEcho/CSF.

Authors' contributions. MH wrote the code for the microcomputers, analysed data, plotted graphs and purchased material. JAC did the experiments, analysed data, drafted figures and wrote the text. Both authors gave final approval for publication and agree to be held accountable for the work.

Competing interests. The authors declare they have no competing interests.

Funding. This work received no external funding.

Acknowledgements. The authors thank David Crofts for gifts of electronic components.

References

1. Tsai PS, Kaufhold JP, Blinder P, Friedman B, Drew PJ, Karten HJ, Lyden PD, Kleinfeld D. 2009 Correlations of neuronal and microvascular densities in murine cortex revealed by direct counting and colocalization of nuclei and vessels. *J. Neurosci.* **29** (46), 14553-14570. Epub 2009/11/20. (doi: 10.1523/JNEUROSCI.3287-09.2009)
2. Motti ED, Imhof HG, Yasargil MG. 1986 The terminal vascular bed in the superficial cortex of the rat. An SEM study of corrosion casts. *J. Neurosurg.* **65** (6), 834-846. Epub 1986/12/01. (doi: 10.3171/jns.1986.65.6.0834)
3. Spector R, Robert Snodgrass S, Johanson CE. 2015 A balanced view of the cerebrospinal fluid composition and functions: Focus on adult humans. *Exp. Neurol.* **273**, 57-68. Epub 2015/08/08. (doi: 10.1016/j.expneurol.2015.07.027)
4. Rasmussen MK, Mestre H, Nedergaard M. 2021 Fluid transport in the brain. *Physiol. Rev.* Epub 2021/05/06. (doi: 10.1152/physrev.00031.2020)
5. Mawuenyega KG, Sigurdson W, Ovod V, Munsell L, Kasten T, Morris JC, Yarasheski KE, Bateman RJ. 2010 Decreased clearance of CNS beta-amyloid in Alzheimer's disease. *Science*. **330** (6012), 1774 (doi: 10.1126/science.1197623)
6. Key A, Retzius G. 1875 Studien in der Anatomie des Nervensystems und des Bindegewebes. Stockholm: Samson & Waller.
7. Rennels ML, Gregory TF, Blaumanis OR, Fujimoto K, Grady PA. 1985 Evidence for a 'paravascular' fluid circulation in the mammalian central nervous system, provided by the rapid distribution of tracer protein throughout the brain from the subarachnoid space. *Brain Res.* **326** (1), 47-63. Epub 1985/02/04. (doi: 0006-8993(85)91383-6 [pii])
8. Kida S, Pantazis A, Weller RO. 1993 CSF drains directly from the subarachnoid space into nasal lymphatics in the rat. Anatomy, histology and immunological significance. *Neuropathol. Appl. Neurobiol.* **19** (6), 480-488. Epub 1993/12/01.
9. Iliff JJ, *et al.* 2012 A paravascular pathway facilitates CSF flow through the brain parenchyma and the clearance of interstitial solutes, including amyloid beta. *Sci. Trans. Med.* **4** (147), 147ra111. Epub 2012/08/17. (doi: 4/147/147ra111 [pii] 10.1126/scitranslmed.3003748)
10. Iliff JJ, Wang M, Zeppenfeld DM, Venkataraman A, Plog BA, Liao Y, Deane R, Nedergaard M. 2013 Cerebral arterial pulsation drives paravascular CSF-interstitial fluid exchange in the murine brain. *J. Neurosci.* **33** (46), 18190-18199. Epub 2013/11/15. (doi: 10.1523/JNEUROSCI.1592-13.2013)
11. Coles JA, Myburgh E, Ritchie R, Hamilton A, Rodgers J, Mottram JC, Barrett MP, Brewer JM. 2015 Intravital imaging of a massive lymphocyte response in the cortical dura of mice after peripheral infection by trypanosomes. *PLoS Negl. Trop. Dis.* **9** (4), e0003714. Epub 2015/04/17. (doi: 10.1371/journal.pntd.0003714)

12. Smith AJ, Yao X, Dix JA, Jin BJ, Verkman AS. 2017 Test of the 'glymphatic' hypothesis demonstrates diffusive and aquaporin-4-independent solute transport in rodent brain parenchyma. *eLife*. **6**. (doi: 10.7554/eLife.27679)
13. Cathélin F. 1903 La circulation du liquide céphalo-rachidien. *C.R. Soc. Biol.* **55**, 1167-1169
14. Yang L, Kress BT, Weber HJ, Thiyagarajan M, Wang B, Deane R, Benveniste H, Iliff JJ, Nedergaard M. 2013 Evaluating glymphatic pathway function utilizing clinically relevant intrathecal infusion of CSF tracer. *J. Trans. Med.* **11** (1), 107. Epub 2013/05/03. (doi: 1479-5876-11-107 [pii] 10.1186/1479-5876-11-107)
15. Ma Q, Ineichen BV, Detmar M, Proulx ST. 2017 Outflow of cerebrospinal fluid is predominantly through lymphatic vessels and is reduced in aged mice. *Nat. Comm.* **8** (1), 1434. Epub 2017/11/12. (doi: 10.1038/s41467-017-01484-6)
16. Zakharov A, Papaiconomou C, Koh L, Djenic J, Bozanovic-Sosic R, Johnston M. 2004 Integrating the roles of extracranial lymphatics and intracranial veins in cerebrospinal fluid absorption in sheep. *Microvasc. Res.* **67** (1), 96-104. Epub 2004/01/08. (doi: S0026286203000736 [pii])
17. Ahn JH*, et al.* 2019 Meningeal lymphatic vessels at the skull base drain cerebrospinal fluid. *Nature*. **572** (7767), 62-66. Epub 2019/07/26. (doi: 10.1038/s41586-019-1419-5)
18. Louveau A*, et al.* 2018 CNS lymphatic drainage and neuroinflammation are regulated by meningeal lymphatic vasculature. *Nat. Neurosci.* **21** (10), 1380-1391. Epub 2018/09/19. (doi: 10.1038/s41593-018-0227-9)
19. Jin BJ, Smith AJ, Verkman AS. 2016 Spatial model of convective solute transport in brain extracellular space does not support a "glymphatic" mechanism. *J. Gen. Physiol.* **148** (6), 489-501. Epub 2016/11/12. (doi: 10.1085/jgp.201611684)
20. Holter KE*, et al.* 2017 Interstitial solute transport in 3D reconstructed neuropil occurs by diffusion rather than bulk flow. *Proc. Natl Acad. Sci.* **114** (37), 9894-9899. Epub 2017/08/30. (doi: 10.1073/pnas.1706942114)
21. Martinac AD, Bilston LE. 2020 Computational modelling of fluid and solute transport in the brain. *Biomech. Model. Mechanobiol.* **19** (3), 781-800. Epub 2019/11/14. (doi: 10.1007/s10237-019-01253-y)
22. Bowsher D. 1957 Pathways of absorption of protein from the cerebrospinal fluid: an autoradiographic study in the cat. *Anat. Rec.* **128** (1), 23-39. Epub 1957/05/01. (doi: 10.1002/ar.1091280104)
23. Wagner HJ, Pilgrim C, Brandl J. 1974 Penetration and removal of horseradish peroxidase injected into the cerebrospinal fluid: role of cerebral perivascular spaces, endothelium and microglia. *Acta Neuropathol.* **27** (4), 299-315. Epub 1974/04/30
24. Pizzo ME*, et al.* 2018 Intrathecal antibody distribution in the rat brain: surface diffusion, perivascular transport and osmotic enhancement of delivery. *J. Physiol.* **596** (3), 445-475. Epub 2017/10/13. (doi: 10.1113/JP275105)
25. Hannocks MJ, Pizzo ME, Huppert J, Deshpande T, Abbott NJ, Thorne RG, Sorokin L. 2018 Molecular characterization of perivascular drainage pathways in the murine brain. *J. Cereb. Metab. Blood Flow*. **38** (4), 669-686. Epub 2017/12/29. (doi: 10.1177/0271678X17749689)
26. Abbott NJ, Pizzo ME, Preston JE, Janigro D, Thorne RG. 2018 The role of brain barriers in fluid movement in the CNS: is there a 'glymphatic' system? *Acta Neuropathol.* **135** (3), 387-407. Epub 2018/02/13. (doi: 10.1007/s00401-018-1812-4)
27. Ma Q, Ries M, Decker Y, Muller A, Riner C, Bucker A, Fassbender K, Detmar M, Proulx ST. 2019 Rapid lymphatic efflux limits cerebrospinal fluid flow to the brain. *Acta Neuropathol.* **137** (1), 151-165. Epub 2018/10/12. (doi: 10.1007/s00401-018-1916-x)
28. Mott FW. 1910 The Oliver-Sharpey Lectures on the cerebro-spinal fluid. Lecture I. *Lancet*. 1-8
29. Mestre H, Mori Y, Nedergaard M. 2020 The Brain's Glymphatic System: Current Controversies. *Trends Neuronsci.* **43** (7), 458-466. Epub 2020/05/20. (doi: 10.1016/j.tins.2020.04.003)
30. Novak U, Kaye AH. 2000 Extracellular matrix and the brain: components and function. *J. Clin. Neurosci.* **7** (4), 280 - 290. (doi: 10.1054/jocn.1999.0212)
31. Sanderson JM, Wright G, Sims FW. 1972 Brain damage in dogs immediately following pulsatile and non-pulsatile blood flows in extracorporeal circulation. *Thorax*. **27** (3), 275-286. Epub 1972/05/01
32. McMaster PD, Parsons RJ. 1938 The effect of the pulse on the spread of substances through tissues. *J. Exp. Med*. **68** (3), 377-400. Epub 1938/08/31
33. Parsons RJ, McMaster PD. 1938 Normal and pathological factors influencing the spread of a vital dye in the connective tissue. *J. Exp. Med.* **68** (6), 869-890. Epub 1938/10/31
34. Ward DD, Ranson JJ, Wallace LMK, Llewellyn DJ, Rockwood K. 2022 Frailty, lifestyle, genetics and dementia risk. *J. Neurol. Neurosurg. Psychiat.* Epub 21 December 2021. (doi: 10.1136/jnnp-2021-327396)

35. Coles JA, Myburgh E, Brewer JM, McMenamin PG. 2017 Where are we? The anatomy of the murine cortical meninges revisited for intravital imaging, immunology, and clearance of waste from the brain. *Prog. Neurobiol.* **156**, 107-148. Epub 2017/05/30. (doi: S0301-0082(16)30053-3 [pii] 10.1016/j.pneurobio.2017.05.002)
36. Darcy H. 1856 Les Fontaines publiques de la Ville de Dijon. Paris: Victor Dalmont. 647 p.
37. Miller-Brownlie TA. 1919 Subsoil water in relation to tube wells. *Indian and Eastern Engineer*. **45**, 191-193
38. Soni JP, Nurul I, Basak P. 1978 An experimental evaluation of non-Darcian flow in porous media. *J. Hydrology*. **38**, 231-241.)
39. Prada A, Civan F. 1999 Modification of Darcy's law for the threshold pressure gradient. *J. Petr. Sci. Eng.* **22** (4), 237 - 240
40. Zeng B, Linsong C, Chunlan L. 2012 Low velocity non-linear flow in ultra low-permeability reservoir. *J. Petr. Sci. Eng.* **80** ((1)), 1-6. (doi: 10.1016/j.petrol.2011.10.006)
41. Levick JR. 1987 Flow through interstitium and other fibrous matrices. *QJ. Exp. Physiol.* **72** (4), 409-437. Epub 1987/10/01. (doi: 10.1113/expphysiol.1987.sp003085)
42. Jones G, Christian SM. 1937 The viscosity of aqueous solutions of electrolytes as a function of the concentration. V. sodium chloride. *J. Am. Chem. Soc.* **59**, 484 - 486
43. Johnson EM, Deen WM. 1996 Hydraulic permeability of agarose gels. *Amer. Inst. Chem. Eng. J*. **42** (5), 1220-1224
44. Pallman H, Deuel H. 1945 Uber die Wasserdurchlässigkeit von Hydrogelen. *Experientia*. **1** (9), 325-326
45. Wang X, Yang Z, Sun Y, Liu X. 2011 Experimental and theoretical investigation of nonlinear flow in low permeability reservoir. *Proc. Env. Sci.* **11**, 1392-1399. (doi: 10.1016/j.proenv.2011.12.209)
46. Cherubini C, Giasi CI, Pastore N. 2012 Bench scale laboratory tests to analyze non-linear flow in fractured media. *Hydrol. Earth Syst. Sci.* **16** (8), 2511-2522. (www.hydrol-earth-syst-sci.net/16/2511/2012)
47. Desai KH, Sato R, Schauble E, Barsh GS, Kobilka BK, Bernstein D. 1997 Cardiovascular indexes in the mouse at rest and with exercise: new tools to study models of cardiac disease. *Am. J. Physiol.* **272**, H1053 - H1061
48. Hladky SB, Barrand MA. 2014 Mechanisms of fluid movement into, through and out of the brain: evaluation of the evidence. *Fluids Barriers CNS*. **11** (1), 26. Epub 2015/02/14. (doi: 10.1186/2045-8118-11-26
114 [pii])
49. Asgari M, de Zelicourt D, Kurtcuoglu V. 2016 Glymphatic solute transport does not require bulk flow. *Sci. Rep.* **6**, 38635. Epub 2016/12/09. (doi: 10.1038/srep38635)
50. Oshio K, Watanabe H, Song Y, Verkman AS, Manley GT. 2005 Reduced cerebrospinal fluid production and intracranial pressure in mice lacking choroid plexus water channel Aquaporin-1. *FASEB J*. **19** (1), 76-78. Epub 2004/11/10. (doi: 04-1711fje [pii]
10.1096/fj.04-1711fje)
51. Rudick RA, Zirretta DK, Hernden RM. 1982 Clearance of albumin from mouse subarachnoid space: a measure of CSF bulk flow. *J. Neurosci. Meth.* **6**, 253-259
52. Liu G, Mestre H, Sweeney AM, Sun Q, Weikop P, Du T, Nedergaard M. 2020 Direct measurement of cerebrospinal fluid production in mice. *Cell Rep*. **33** (12), 108524. Epub 2020/12/29. (doi: 10.1016/j.celrep.2020.108524)
53. Vincent TJ, Thiessen JD, Kurjewicz LM, Germscheid SL, Turner AJ, Zhilkin P, Alexander ME, Martin M. 2010 Longitudinal brain size measurements in APP/PS1 transgenic Mice. *Mag. Res. Insights*. **4**, 19-26. (doi: 10.4137/MRI.S5885)
54. Mann JD, Butler AB, Rosenthal JE, Maffeo CJ, Johnson RN, Bass NH. 1978 Regulation of intracranial pressure in rat, dog, and man. *Ann. Neurol.* **3** (2), 156-165. Epub 1978/02/01. (doi: 10.1002/ana.410030212)
55. Chiu C, Miller MC, Caralopoulos IN, Worden MS, Brinker T, Gordon ZN, Johanson CE, Silverberg GD. 2012 Temporal course of cerebrospinal fluid dynamics and amyloid accumulation in the aging rat brain from three to thirty months. *Fluids Barriers CNS*. **9** (1), 3. Epub 2012/01/25. (doi: 10.1186/2045-8118-9-3)
56. Karimy JK, Kahle KT, Kurland DB, Yu E, Gerzanich V, Simard JM. 2015 A novel method to study cerebrospinal fluid dynamics in rats. *J. Neurosci. Meth.* **241**, 78-84. Epub 2015/01/03. (doi: 10.1016/j.jneumeth.2014.12.015)

57. Mink JW, Blumenschine RJ, Adams DB. 1981 Ratio of central nervous system to body metabolism in vertebrates: its constancy and functional basis. *Am. J. Physiol.* **241** (3), R203-212. Epub 1981/09/01. (doi: 10.1152/ajpregu.1981.241.3.R203)
58. Boero JA, Ascher J, Arregui A, Rovainen C, Woolsey TA. 1999 Increased brain capillaries in chronic hypoxia. *J. App. Physiol.* **86** (4), 1211-1219. Epub 1999/04/08. (doi: 10.1152/jappl.1999.86.4.1211)
59. Hudetz AG. 1997 Blood flow in the cerebral capillary network: a review emphasizing observations with intravital microscopy. *Microcirculation*. **4** (2), 233-252. Epub 1997/06/01.)
60. Pawlik G, Rackl A, Bing RJ. 1981 Quantitative capillary topography and blood flow in the cerebral cortex of cats: an in vivo microscopic study. *Brain Res*. **208** (1), 35-58. Epub 1981/03/09
61. Nishimura C, Polesskaya O, Dewhurst S, Silva JN. 2016 Quantification of cerebral vascular architecture using two-photon microscopy in a mouse model of HIV-induced neuroinflammation. *J. Vis. Exp.* (107), e53582. Epub 2016/02/11. (doi: 10.3791/53582)
62. Reese TS, Karnovsky MJ. 1967 Fine structural localization of a blood-brain barrier to exogenous peroxidase. *J. Cell Biol.* **34** (1), 207-217. Epub 1967/07/01. (doi: 10.1083/jcb.34.1.207)
63. Thomsen MS, Routhe LJ, Moos T. 2017 The vascular basement membrane in the healthy and pathological brain. *J. Cereb. Metab. Blood Flow*. **37** (10), 3300-3317. Epub 2017/07/29. (doi: 10.1177/0271678X17722436)
64. Ceafalan LC, Fertig TE, Gheorghe TC, Hinescu ME, Popescu BO, Pahnke J, Gherghiceanu M. 2019 Age-related ultrastructural changes of the basement membrane in the mouse blood-brain barrier. *J. Cell. Mol. Med.* **23** (2), 819-827. Epub 2018/11/20. (doi: 10.1111/jcmm.13980)
65. Burns SA, Elsner AE, Gast TJ. 2021 Imaging the Retinal Vasculature. *Ann. Rev. Vis. Sci.* **7**, 129-153. Epub 2021/06/26. (doi: 10.1146/annurev-vision-093019-113719)
66. Xie L, *et al.* 2013 Sleep drives metabolite clearance from the adult brain. *Science*. **342** (6156), 373-377. Epub 2013/10/19. (doi: 10.1126/science.1241224)

Supplementary Material

SM1. Detailed Methods
SM2. Pulsation reduces transport of a solute through an open flexible tube

SM1. Detailed Methods

1.1. Gel columns.

400 mg of agar agar (Top Op Foods Ltd, Stanmore, UK), was added to 40 ml of 0.15 M NaCl in a beaker which was warmed in a water bath at about 90 ºC. The mixture was stirred for 30 min. A10 ml syringe with a 19G needle, shortened and blunted with a diamond file, was used to inject columns of the warm agar into several 40 - 80 mm lengths of the silicone tubing i.d. 1.0 mm, o.d. 3.0 mm. The filled tubes were then stored in 0.15M NaCl at room temperature for up to a week.

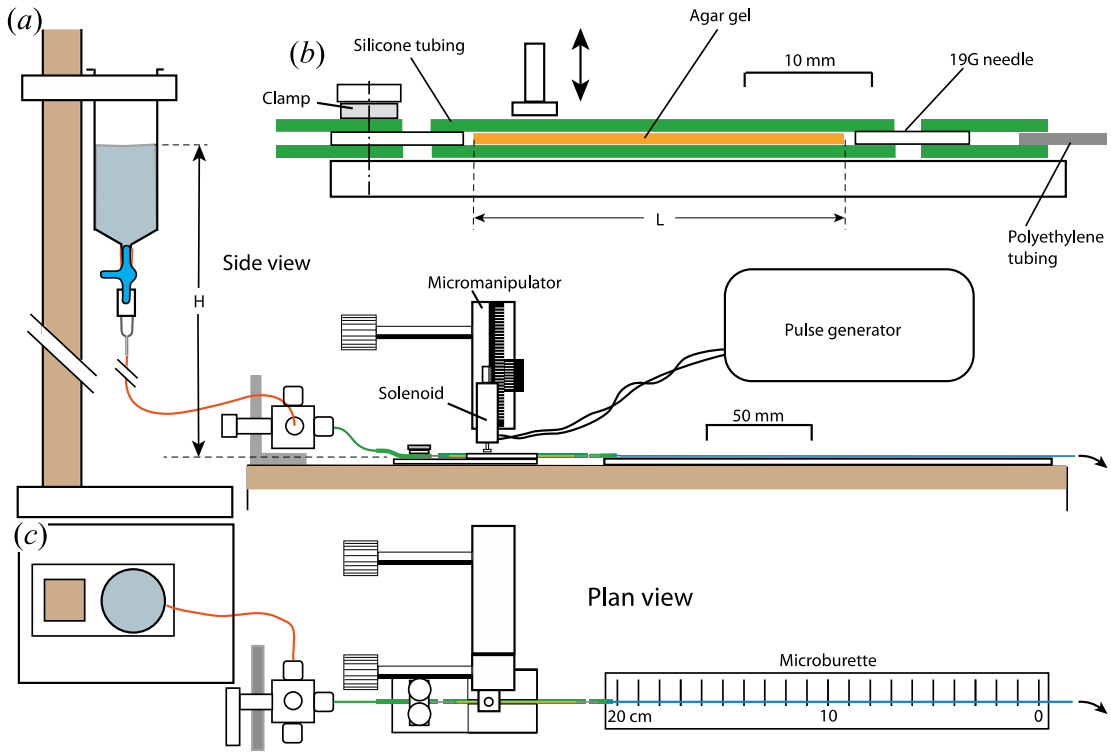

Figure SM1. The apparatus. (*a*) side view, (*c*) plan view. (*b*) Enlargement showing the gel column under the solenoid and the connections to the inflow and the microburette.

1.2. Apparatus for flow measurement

As shown in Fig. SM1(a), to apply a longitudinal pressure gradient to the gel-filled tube, a filter stand was used to support a reservoir (a 50 ml syringe) containing 0.15 M NaCl with its surface at a height H above above the horizontal gel-filled tube. H was set at 200, 300, 400 or 500 mm. The fluid was led through a four-way distribution valve (HVP 86788, Hamilton, Bonaduz, CH) to 1 mm i.d. silicone tubing then the gel column, then a microburette consisting of low density polyethylene tubing (Portex, Smith Medical) with a nominal internal diameter of 0.38 mm, held with sellotape along 200 mm of a ruler scale.

1.3. Mounting the gel column

The silicone tube containing gel was cut to 10 mm longer than the desired length, *L*, of column. The 29G needle of an insulin syringe was cut to 5 mm with a diamond file and filled with 0.15M NaCl. It was inserted in each end of a length of tube and gel was flushed out and replaced by the saline solution. The tube from the reservoir ended in a length of 19G needle (Fig. SM1(*b*)); saline was allowed to flow until the needle was full; then the tip of the needle was inserted in one end of the gel tube. To avoid pressure on the gel, the distribution valve was turned to an open port and the needle further inserted to about 4 mm. Similarly, a length of 19G needle was inserted in the downstream end of the gel tube. This led to another length of 1 mm silicone tubing, which was filled with saline, and brought up to the microburette tubing, which was also full. When the microburette tube was pushed into the silicone tube, a bubble invariably entered it and was driven a short way down the scale. The advancing position of the downstream end of this bubble, best seen with torchlight and a loupe, was used

to measure the flow. The timing between measurements was chosen so that the displacement was at least 1 mm: for overnight runs it could be more than 50 mm.

1.4. The solenoid.

A 5 V solenoid (The Pi Hut, SKU:ADA2776) with a piston diameter of 3.5 mm was held vertically above the gel tube on a micromanipulator, about 10 mm from its upstream end. Its vertical position was determined to 0.1 mm with a Vernier scale. It's current was switched by a transistor (BFY51) controlled by a Raspberry Pi zero microcomputer. Although the duty cycle could be varied, it was kept at 50%. The Raspberry Pi was controlled by wifi from a MacBook Pro using the program 'Solenoid.py' on https://github.com/GolfPapaEcho/CSF.

SM2. Pulsation reduces transport of a solute through an open flexible tube.

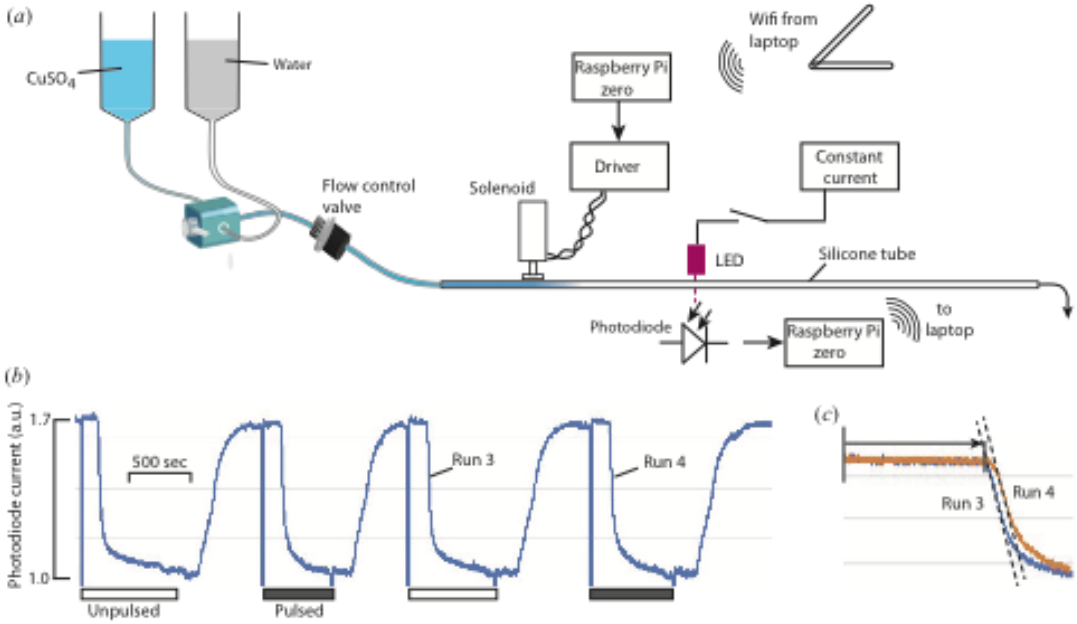

Figure SM2. (*a*) Scheme for measuring the transport of a solute along an elastic tube. The photodiode was about 20 cm downstream of the two-way valve. Flow control valve: Biorad FCV. (*b*) When the solution was switched from water to $CuSO_4$ solution (bars) the photodiode current fell after a delay. Filled bars indicate that the solenoid was activated at 5 Hz, 50% dury cycle. (*c*) Superimposed traces of two runs in (*b*) illustrating how, on average, the transport of $CuSO_4$ was delayed when the tube was pulsed.